JOURNAL OF SOLID STATE CHEMISTRY 76, 7–17 (1988)

Structural, Thermal, and Transport Studies on Silver Vanadium Phosphate Solid Electrolyte

P. SATHYA SAINATH PRASAD AND S. RADHAKRISHNA

Departments of Physics, Indian Institute of Technology, Madras 600 036, India

Received December 1, 1987; in revised form February 16, 1988

Silver-based quarternary fast ion conducting polycrystalline and glassy materials have been prepared by the open-air crucible melting method. A preliminary investigation revealed that the glassy electrolyte, when used in an electrochemical cell, has a high capacity of 15 mAH for the composition mole% 66.6 AgI–22.2 Ag_2O–11.1 (0.8 V_2O_5–0.2 P_2O_5). In a further study, to establish the highest conducting composition, by varying the AgI mole%, it was found that the composition with mole% 70 AgI–20 Ag_2O–10 (0.8 V_2O_5–0.2 P_2O_5) has an ionic conductivity of 8.2×10^{-2} (ohm cm)$^{-1}$ and an electronic conductivity of 2.6×10^{-8} (ohm cm)$^{-1}$ at 32°C. The infrared, far infrared, Raman, and EPR spectroscopic techniques were used to analyze and confirm the presence of ionic clusters, thus highlighting the structural units of the solid electrolyte. The existence of ionic clusters in the glass was assumed to be responsible for enhanced ionic conduction. Thermal and transport properties of the compound were studied to explore the effect of mixing two glass formers. The glass transition temperature (T_g) obtained from the DTA technique was well correlated with the obtained glass transition temperature from the log σT vs $10^3/T$ plot. The resistance–time and the resistance–frequency characteristics of the pellets were investigated to study the behavior of the material as an electrolyte in solid-state batteries.

1. Introduction

In search of silver-based superionic conducting materials to be used as electrolytes in solid-state batteries and analog memory devices, efforts are being channeled to develop vitreous electrolytes with an ionic conductivity of 0.1 ohm^{-1} cm^{-1} at room temperature (32°C). The silver-based ternary systems AgI–Ag_2O–V_2O_5 and AgI–Ag_2O–P_2O_5 were well studied and reported (*1–3*). On the assumption that a mixture of two glass formers will be a better glass former with an enhancement in ionic conduction due to the increased randomness in glassy matrix and the formation of ionic clusters due to the difference in ionic radii and electropositivity of the glass former cations, a new quarternary system with Ag_2O as glass modifier and V_2O_5, P_2O_5 as glass formers was studied (*4*). The glass with mole% 66.6 AgI–22.2 Ag_2O–11.1 (0.8 V_2O_5–0.2 P_2O_5) composition has an ionic conductivity of 4.2×10^{-2} ohm^{-1} cm^{-1} and an electronic conductivity of 1.8×10^{-10} ohm^{-1} cm^{-1} at room temperature. In the present work, the AgI content is varied from 40 to 85 mole% in the above indicated glass, keeping the glass modifier to glass former ratio and the two glass formers ratio the same. On investigation of the variation of ionic conductivity with AgI mole% and establishment of the glass-forming region, it was found that the glass with composition

0022-4596/88 $3.00

mole% 70 AgI–20 Ag_2O–10 (0.8 V_2O_5–P_2O_5) coded as 70VP82G has the highest ionic conductivity of 8.2×10^{-2} ohm^{-1} cm^{-1} at 32°C which is close to that of superionic conducting AgI (*5*).

2. Experimental

2.1 Method of Preparation

The three methods of preparation of glasses were explained in detail in a previous communication (*4*). It was shown that open-air crucible melting and rapid quenching method have an advantage over the other two methods as described therein. The appropriate amounts of analar-grade compounds AgI, Ag_2O, V_2O_5, and P_2O_5 corresponding to mole% 70 AgI–20 Ag_2O–10 (0.8 V_2O_5–0.2 P_2O_5) were taken in a quartz crucible and heated in an electric muffle furnace at 600°C for 3 hr. One-half of the homogeneous melt was rapidly quenched in liquid nitrogen column and the other half was allowed to cool down slowly to room temperature. Both the samples were prepared from the same melt so as to compare their properties without any ambiguity in their composition and thermal history.

2.2 XRD and DTA

X-ray diffractograms were recorded on 1.0 g of the pulverized samples using Philips PW-1130 X-ray generator with a Model PW-1050 vertical diffractometer and a PW-1710 control unit. The radiation used was Cu$K\alpha$ with a nickel filter for 35 kV and 25 mA.

Since DTA is generally considered to be a sensitive recorder of a structural change; it was thought worthwhile to examine the stability of the prepared samples which can be used as electrolytes. Thus the differential thermal analysis was carried out using a DuPont 900 DSC instrument.

2.3 Ionic and Electronic Conductivities

Pulverized samples were pressed to form cylindrical pellets of diameter 1.3 cm of the configuration (Ag)/(Sample)/(Ag) together with electrode mixture of 200-mesh silver powder and sample powder in 2 : 1 ratio by weight under a uniform pressure of 6000 kg/cm^2 using a Perkin–Elmer handpress. The mixture of sample powder silver electrodes were used for a better electrode–electrolyte contact. Ionic conductivity measurements were undertaken on those resulting pellets of 1.3 cm diameter, using a General Radio bridge Model 1650 B, with an internal oscillator at 1.0 kHz and a null detector, in the temperature range 305–405°K.

Electronic conductivity measurements were carried on the polarization cell of the configuration (−)Ag/Sample/Graphite(+) as described by Wagner (*5*). Various dc potentials less than the decomposition potential of the electrolyte were applied and the corresponding currents after steady state were noted using a Keithley 610C electrometer.

2.4 Infrared and Far Infrared Absorption Spectra

The pulverized samples were dispersed in spectral-grade KBr powder and the transmission spectra in the infrared region 4000–400 cm^{-1} were recorded on a Perkin–Elmer 839 IR spectrophotometer. Far IR spectra were recorded on samples dispersed in polyethylene using a Polytec 30 Fourier spectrometer with a far IR Michelson interferometer, in the region 500–50 cm^{-1}.

2.5 EPR and Raman Spectra

A Varian E4 X-band spectrometer operating at 9 GHz with a variable temperature accessory was used to record EPR spectra. Raman spectra were recorded on a small piece of the sample glass using a Cary 82

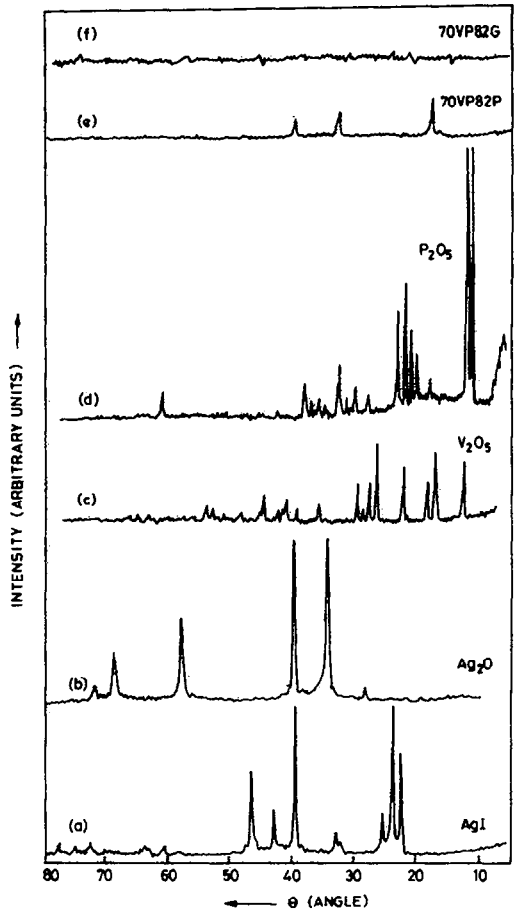

FIG. 1. X-ray diffractogram of (a) AgI, (b) Ag_2O, (c) V_2O_5, (d) P_2O_5, (e) polycrystalline 70VP82, and (f) amorphous 70VP82 material.

spectrometer coupled with a Spectra Physics krypton ion laser operating at 0.2 W at 6471 Å wavelength.

3. Results and Discussion

3.1 XRD and DTA

Figure 1 shows the X-ray diffractograms for the samples prepared as described before along with those of AgI, Ag_2O, V_2O_5, and P_2O_5. In the rapid quenching case the XRD (Fig. 1f) confirms the amorphous nature of the obtained material. In the other case, formation of a new polycrystalline compound with slight traces of AgI which is different from the basic compounds AgI, Ag_2O, V_2O_5, and P_2O_5 was observed.

From the XRD, only the vitreous nature can be predicted, whereas to compare them out of thermodynamic equilibrium a DTA has to be performed to establish the glass transition temperature (T_g) and crystallization temperature (T_c). The significance of T_g is due to its relation to the kinetic parameters and the duration of the experiment log σT vs $10^3/T$. On a microscopic level, T_g corresponds to the time required by the elements of the macromolecular chains constituting a glass to move a distance comparable to their size. Thus thermal characterization of a material is very important to study T_g, which reflects the degree of freedom of the macromolecules in the glassy matrix. The analysis developed by Gibbs *et al.* (*6*), Dimarzio and Gibbs (*7*), and then by Adams and Gibbs (*8*) associates the ideal glass transition temperature with the structural relaxation time of the macromolecular chains proportional to $\exp(-W/R(T - T_0))$, where W is the activation energy and T_0 the temperature below which the properties of liquid cannot be extrapolated.

Figure 2 shows the typical DTA trace for polycrystalline and glassy samples in the temperature region 30–400°C. An endothermic peak was observed at 72°C for the glass which is attributed to the glass transition temperature. At a temperature of 120°C, a weight loss of 0.012 mg (not shown in the figure) was observed which might be due to the nucleation of crystallization of the glassy sample. The endothermic inflection at 380°C is due to the absorption of thermal energy by the resulted polycrystalline compound to melt into liquid state. Qualitatively the glassy material appears to possess greater stability to moisture than the polycrystalline material. After the exposure of glass to the laboratory atmosphere for 120 days those additional endothermic peaks were not observed (*9*).

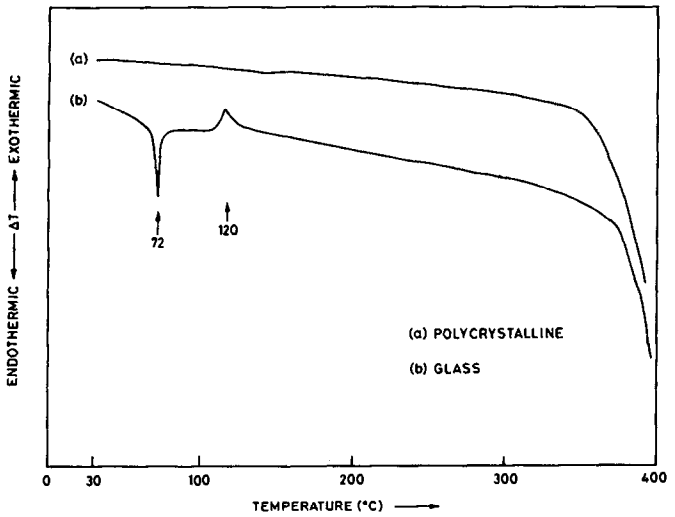

FIG. 2. DTA curve of (a) 70VP82P and (b) 70VP82G with indication of T_g and T_c.

3.2 Ionic Conductivity

Figure 3 indicates the time dependence of the resistance for both polycrystalline and glassy materials. It can be seen as almost independent in the case of the polycrystalline sample whereas it is highly dependent for the glassy sample which can be due to the relaxation and homogenization of charge carriers. Figures 4 and 5 show the variation of $\log \sigma T$ with the inverse of absolute temperature for both glassy and polycrystalline samples, respectively. The glassy sample obeys the Arrhenius relation (*4*) until the glass transition temperature (T_g) and the activation energy is calculated to be 0.264 eV. The observed T_g value was well correlated with that obtained from the DTA technique. Figure 5 has two linear re-

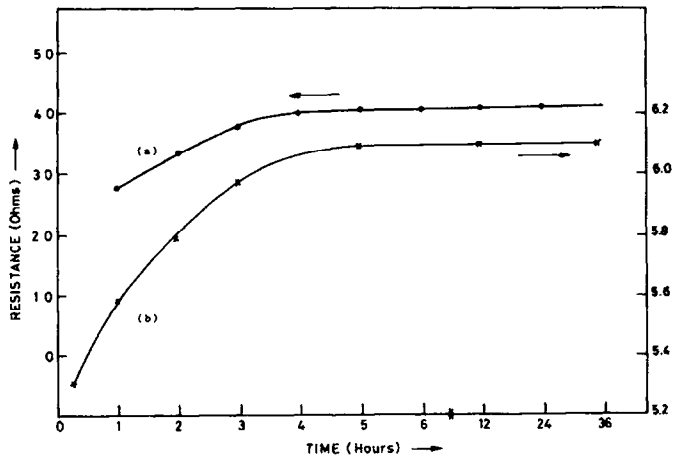

FIG. 3. The variation of resistance with time for (a) polycrystalline and (b) amorphous 70VP82 sample pellets.

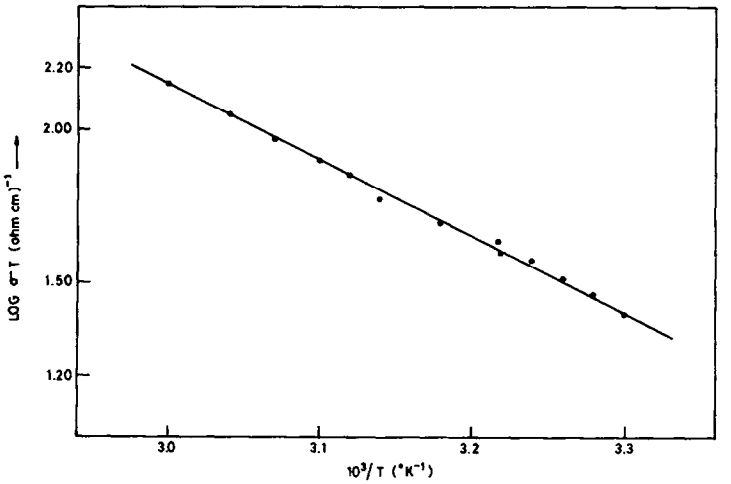

FIG. 4. Plot of log σT vs $10^3/T$ for the amorphous material pellet 70VP82.

gions with activation energies 0.289 and 0.221 eV. This can be explained as follows: At low temperatures, the existence of grain boundaries limits the conduction or migration of ions whereas at high temperatures the tendancy is more for polycrystalline material to become a random network structure, which enhances the ionic conductivity with low activation energy for ion migration. Figure 6 shows the dependence of conductivity on the frequency for the glassy sample which is somewhat different from the other superionic glasses (*10, 11*). At 100 Hz the conductivity is minimum and the observation of a linear dependence in the low-frequency region might be due to the space charge polarization or an interfacial effect. No frequency-dependent conductivity was observed for the polycrystalline material.

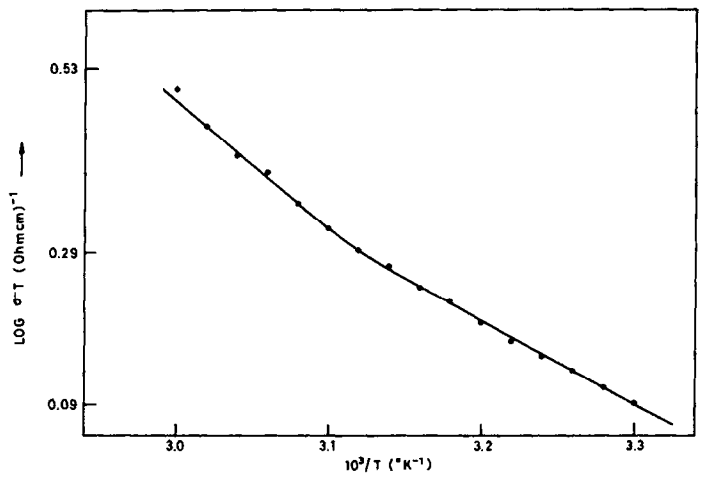

FIG. 5. Plot of log σT vs $10^3/T$ for the polycrystalline material 70VP82 pellet.

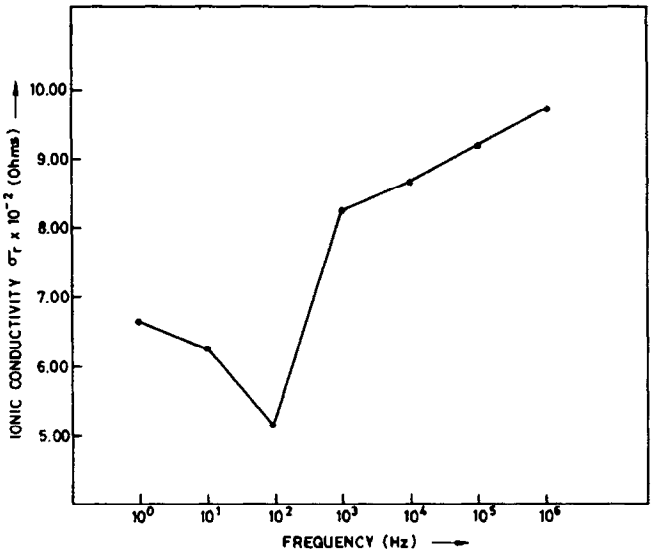

FIG. 6. Frequency dependence of conductivity for the amorphous material 70VP82.

3.3 Electronic Conductivity

Figures 7 and 8 show the *I-V* characteristic curves for both polycrystalline and glassy samples, respectively. The saturation of current at higher applied potentials indicates that the conduction is due only to the electrons but not to electron holes. The original Wagner expression (*12*) for electronic current is

$$I = I_e \approx (RTA/LF)\,\sigma_e\{1 - \exp(-EF/RT)\},$$

where L and A are the length and area of the sample, T the absolute temperature, R the gas constant, F the Faraday's constant, and σ_e is the conductivity due to electrons.

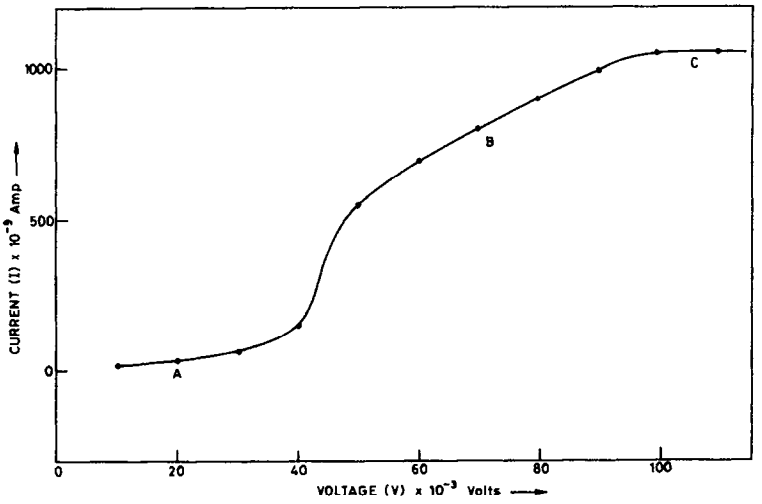

FIG. 7. Current–voltage characteristic curve for the polycrystalline pellet 70VP82.

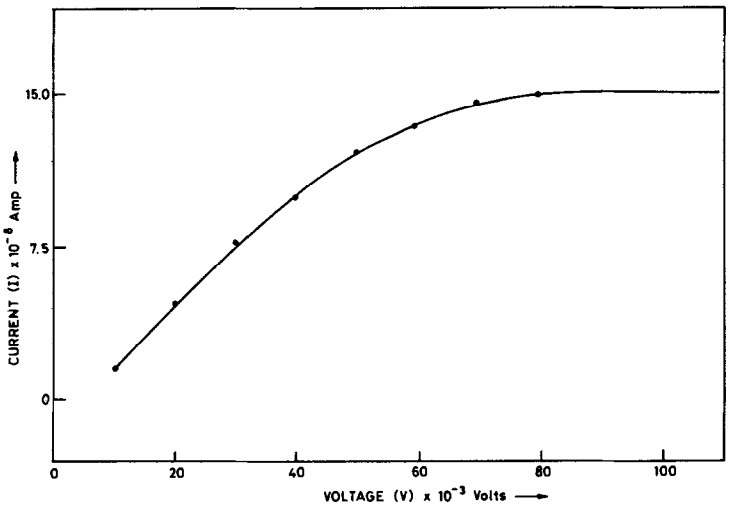

FIG. 8. Current–voltage characteristic curve for the amorphous pellet 70VP82.

When $EF \gg RT$, then

$$I \approx I_e = (RTA/LF)\,\sigma_e.$$

Using the above expression the electronic conductivity was calculated by calculating the saturation current (I_e) from I–V plots. These values are well correlated with those calculated by substituting the slopes of the plots I vs 1-exp($-EF/RT$) and they were found to be 8.10×10^{-8} ohm^{-1} cm^{-1} and 6.2×10^{-6} ohm^{-1} cm^{-1}, respectively.

3.4 IR Studies

The IR spectra of both glass and polycrystalline samples are shown in Fig. 9 and seem to be difficult to interpret. In poly-

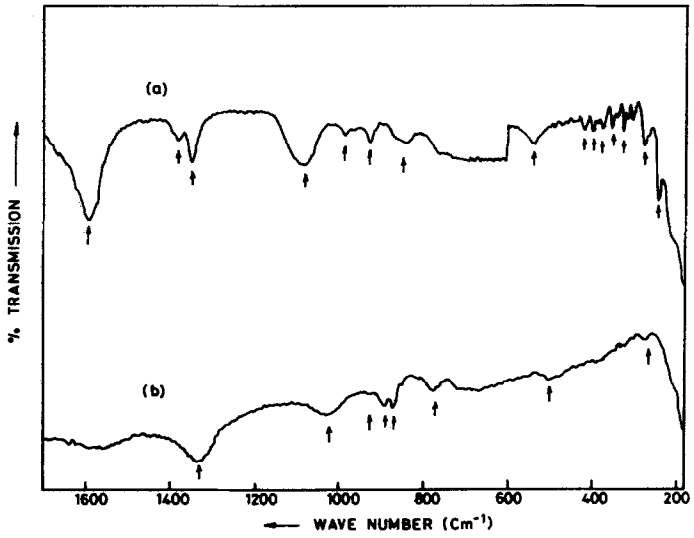

FIG. 9. IR spectra of (a) polycrystalline sample 70VP82 and (b) amorphous 70VP82 in the spectral region 1600–200 cm^{-1} in a KBr matrix.

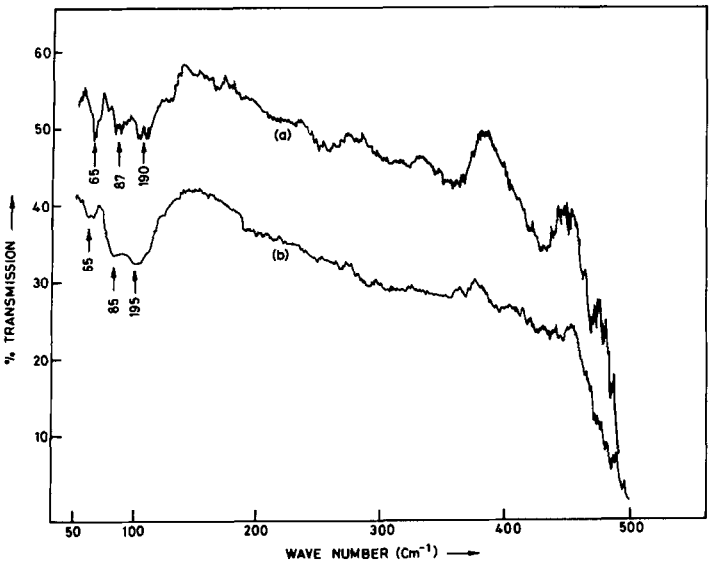

FIG. 10. FIR spectra of (a) polycrystalline sample 70VP82 and (b) amorphous sample 70VP82 dispersed in polyethylene matrix in the region 500–50 cm^{-1}.

crystalline spectra clear broad peaks were observed whereas in glassy spectra the bands are not clear but the peaks are very sharp, which confirms the glassy nature of the material. Well-defined bands with peaks at 1600, 1380, 1350, 1080, 990, 850, 540, and 420 cm^{-1} were observed for the polycrystalline sample and were assigned to particular vibrations by comparing this spectra with those of the features observed in the putative model compounds. Several peaks appearing on the high-frequency side were due to the splitting of V_2O_5 ion frequencies and the appearance of other resolved frequencies were due to phosphate units. The absorption peaks in the range lower than 540 cm^{-1} were due to the deformation of V–O–V linkages and in the region 850 cm^{-1} were due to the formation of P=O bonds and VO_4-like units. By comparing the IR spectra of polycrystalline material with that of glassy material and considering the vibrational shifts due to the vitreous nature, it can be concluded that the glass consists of ionic clusters of PO_4^{3-}, VO_4^{3-}, and their combinations. Thus, from the IR studies, these glasses can be classified as ionic glass rather than condensed glass.

3.5 FIR Studies

The absence of long-range order and the randomness in the skeleton glassy structure may contribute to the mobility of Ag^+ ion through the ionic clusters formed due to different polarizing species V_2O_5 and P_2O_5. Because of the local diffusive motion, the glassy network provides open channel-like pathways for the mobile ions.

Figures 10a and 10b show the FIR spectra of polycrystalline and glassy material, respectively. In Fig. 10a, three bands at 195, 85, and 65 cm^{-1} were observed which are clear when compared to the bands at 190, 87, and 65 cm^{-1} in Fig. 10b. The nature of these bands reflects the state of disorder of AgI in the glassy matrix. The band at 65 cm^{-1} is assigned to the E-symmetry of the Ag^+ ion. The band at 87 cm^{-1} corresponds to Ag^+–I^- vibrations whose intensity increases with AgI content in the glassy ma-

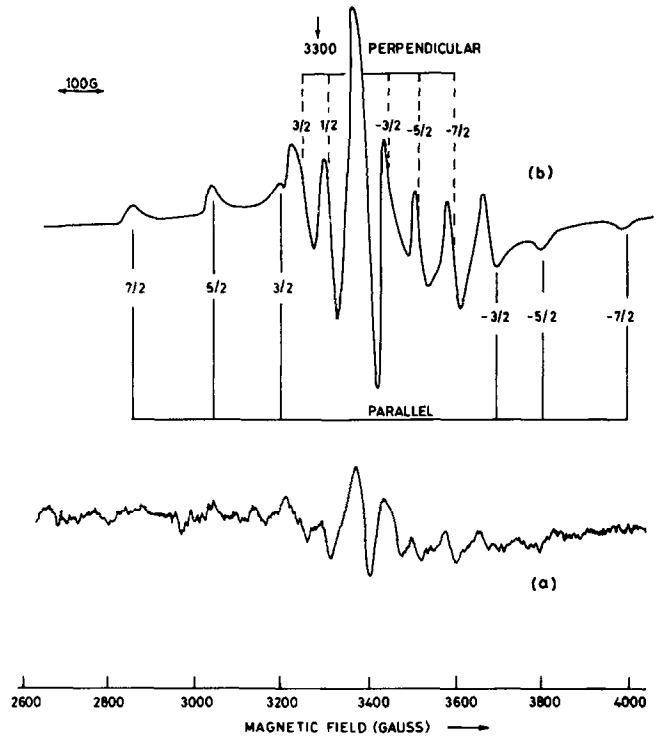

FIG. 11. Electron paramagnetic resonance spectra of (a) polycrystalline 70VP82 and (b) amorphous 70VP82 samples.

trix. Thus the conductivity also increases with AgI content and reaches a maximum at 70 mole%, which supports the contribution from Ag^+ ion in AgI more than the covalently connected Ag^+ ion in Ag_2O.

3.6 EPR Studies

The EPR technique has been used to obtain the concentration of V^{4+}/V^{5+} in the sample. The existence of vanadium in two different valence states in equivalent positions in the VO_6 octahedra linked as chains or sheets was believed to provide continuous path for electronic conduction in semiconducting V_2O_5–P_2O_5 glasses as suggested and supported by Verwey *et al.* (*13*), Ioffe *et al.* (*14*), and Reuter *et al.* (*15*). Typical EPR spectra of both glassy and polycrystalline materials were shown in Figs. 11a and 11b, respectively. The spectrum in Fig. 11a resolves into five perpendicular components and six parallel components for different values of m_I ($-7/2$ to $+7/2$) for vanadyl ion in the form of VO_4^{4-} tetrahedra and $V_2O_6^{4-}$ octahedra. The spin Hamiltonian parameters for the V_2O_5–P_2O_5 semiconducting glass and mole% 70 AgI–20 Ag_2O–10 (0.8 V_2O_5–0.2 P_2O_5) glass are given in Table I. It is evident that the A values are approximately the same, which clearly indicates that the species responsible for the electronic conductivity are the same in both V_2O_5–P_2O_5 and AgI–Ag_2O–V_2O_5–P_2O_5 glasses. However, the difference in the g values indicates a change in the "order" of the system. The near isotropic value of g ($g_I = 1.986$ and $g_{II} = 1.978$) in the present investigation predicts a high ordering of the conducting species when compared to those ($g_I = 2.00$ and $g_{II} = 1.95$) of the semiconducting glasses.

Comparison of the intensities of the EPR

TABLE I

THE CALCULATED SPIN HAMILTONIAN PARAMETERS FROM THE RECORDED EPR SPECTRA OF SEMICONDUCTING 80% V_2O_5–20% P_2O_5 GLASS AND THE SUPERIONIC CONDUCTING 70VP82G

Spin Hamiltonian parameter	80% V_2O_5–20% P_2O_5 semiconducting glass	70VP82G superionic conducting glass
$g_{\parallel}$	1.950	1.978
$g_{\perp}$	2.000	1.986
$A_{\parallel}$	160 ± 2	160 ± 5
$A_{\perp}$	72 ± 2	70 ± 2

spectra in Figs. 11a and 11b indicates that the concentration of vanadium in 4+ state is high in the polycrystalline sample than in the glassy sample. Thus a high electronic conductivity was observed in the polycrystalline, since V^{4+}/V^{5+} partial valence mechanism is responsible for the electronic conductivity. From the near isotropic nature of the g values for glassy material, it was evident that a glass modifier (Ag_2O) brings "order" to the glassy matrix containing V_2O_5 and P_2O_5 structural units, thus aiding ionic conductivity and reducing the electronic conductivity drastically.

3.7 Raman Studies

The motion of mobile ions in superionic conductors is associated with stray moments which can interact with the electric field of incident electromagnetic radiation of proper polarization. A change in the Raman shift for the pure AgI and the glass would be consistent with the anion entering vacant sites of the macromolecular structure. If the Raman spectrum does not show any modification of the P–O or V–O vibrational modes upon the addition of large quantities of silver iodide, then free anions and cations may exist and transport might be fit into the free ion model introduced by Rice and Roth (*16*).

The Raman spectrum at room temperature for the glassy material in the form of a small cube is shown in Fig. 12. Five bands exist at 87, 120, 250, 340, and 420 cm^{-1} in

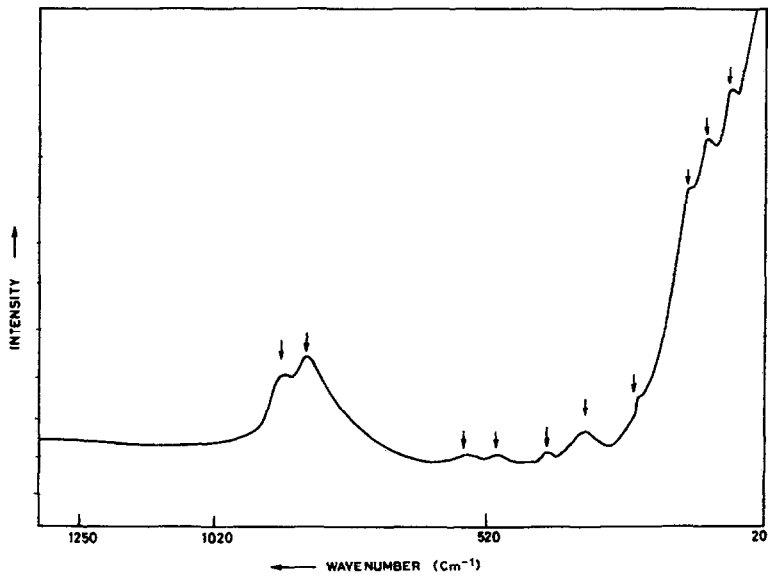

FIG. 12. Raman spectra of a small glass cube 5 × 5 × 5 mm dimensions in the wave number region 1250–20 cm^{-1} on interaction with 6471 Å line of krypton ion laser.

the higher region and four bands exist at 500, 540, 850, and 890 cm^{-1} in the lower region. Comparing the IR and FIR spectra with the Raman spectrum for the glassy material; it can be concluded that the band at 87 cm^{-1} is both IR and Raman active whereas the band at 120 cm^{-1} is only Raman active. The other two bands observed in the FIR at 190 and 65 cm^{-1} were not observed in Raman, hence they are IR active. The Raman bands at 500 and 890 cm^{-1} are due to the $(PO_4)^{3-}$ ionic clusters which are IR active also, whereas the bands at 540 and 850 cm^{-1} are Raman active only. Thus the Raman spectra supplement the IR data.

4. Conclusions

The existence of ionic clusters inferred from spectroscopic studies is assumed to be responsible for high Ag^+ ion conduction, by providing open channel-like pathways for Ag^+ ion migration. Transport studies further support this high Ag^+ ion conductivity in the mole% 70 AgI–20 Ag_2O–10 (0.8 V_2O_5–0.2 P_2O_5) material. The observed low electronic conductivity in glasses satisfies the requirement for a good solid electrolyte in increasing the shelf life of a battery by decreasing the self-discharge. So this material can be used as solid electrolyte in solid-state batteries.

Acknowledgment

One of the authors (P.S.S.N.P.) thanks Dr. N. Sreehari of RSIC, IIT, Madras for his kind help in the analysis and correlation of spectroscopic studies with transport measurements.

References

1. T. Minami, Y. Takuma, and M. Tanaka, *J. Electrochem. Soc.* **124,** 1659 (1977).
2. T. Minami, K. Imazawa, and M. Tanaka, *J. Non-Cryst. Solids* **42,** 469 (1980).
3. K. Hariharan, R. Kaushik, and S. Radhakrishna, "Materials for Solid State Batteries" (B. V. R. Choudari, Ed.), World Scientific, Singapore (1986).
4. P. Sathya Sainath Prasad and S. Radhakrishna, *J. Mater. Sci. Lett.* (1988), in press.
5. W. Wagner, *J. Electrochem. Soc.* **6,** 128 (1981).
6. J. H. Gibbs *et al.*, *J. Chem. Phys.* **28,** 373 (1958).
7. E. A. Dimarzio and J. H. Gibbs, *J. Chem. Phys.* **28,** 807 (1958).
8. G. Adam and J. H. Gibbs, *J. Chem. Phys.* **43,** 139 (1965).
9. P. Sathya Sainath Prasad and S. Radhakrishna, *J. Mater. Sci. Lett.* (1988), in press.
10. R. J. Grant, M. D. Ingram, *et al.*, *J. Chem. Phys.* **82,** 2838 (1978).
11. J. Kawamura and M. Shimoji, *J. Non-Cryst. Solids* **79,** 367 (1986).
12. W. Wagner, *J. Electrochem. Soc.* **6,** 128 (1981).
13. E. J. W. Verwey, P. W. Haaijman, *et al.*, *Philips Res. Rep.* **5,** 173 (1950).
14. V. A. Ioffe, I. V. Patrina, and S. V. Poberovskaya, *Sov. Phys. Solid State* **2,** 609 (1960).
15. B. Reutor, J. Jaskowsky, and E. Riedel, *Z. Electrochem.* **63,** 937 (1959).
16. M. J. Rice and W. C. Roth, *J. Solid State Chem.* **4,** 294 (1972).